

Material design and processing of a new class of titanium boride cermets with tough metallic phases and mechanical properties

Alexander Lark, Jun Du, and K.S. Ravi Chandran^{a)}

Department of Metallurgical Engineering, The University of Utah, Salt Lake City, Utah 84112, USA

(Received 27 June 2018; accepted 14 September 2018)

The design and the processing of a new class of titanium boride (TiB)-based bulk cermets containing a metallic phase (β -Ti phase) for toughening is presented. The general approach is rapid reaction and densification, using starting powders of Ti, TiB₂, Fe, and Mo, by electric-field-activated sintering. The cermets consist of two-phase microstructures in which the boride phase formed as a networked structure of TiB whiskers that were created in situ upon the reaction between the powders. Hardness, flexural strength, and fracture toughness measurements of these materials revealed that they possess an interesting set of properties up to: hardness values of 1090 kg/mm², flexural strength values of 953 MPa, and fracture toughness values of 18 MPa m^{1/2}. A remarkable finding is that although the metallic phase fractured by microscopic cleavage, the cermets showed good fracture toughness values. The present study not only illustrates the process details and microstructure leading to these properties but also provides a broad powder metallurgical approach to design and synthesize cermets that may yield further improved properties.

I. INTRODUCTION

Cermets are composites consisting of a ceramic phase that provides hardness and strength and a metallic phase that provides ductility and toughness while structurally ‘binding’ the ceramic phase together. The metallic phase is usually limited to $<0.3 V_f$ (V_f = volume fraction) and is distributed discontinuously within the ceramic phase. Some well-known examples are tungsten carbide (WC) cermets liquid-phase sintered with Co or other metal phases,^{1,2} titanium carbide (TiC) sintered with Fe or Fe-based intermetallics,^{3–5} and titanium carbonitride (TiCN) cermets, sintered with compatible metallic phases.⁶ Among these, the microstructure and mechanical properties of WC-Co cermets have been extensively investigated^{7–9} and this class represents the most widely manufactured material for tools in cutting and drilling applications. In general, the cermet processing is done by liquid phase infiltration or sintering at very high temperatures, where the wettability of the carbide(s) and/or their reaction with the metal phase^{10,11} are critical aspects controlling the mechanical quality of the cermets.

We present here a new direction in the processing of cermets, where the titanium boride (TiB)-based cermet is created in situ by reaction sintering of powders under the heating induced by the electric field. The in situ reaction produces a two-phase mixture of TiB and β -Ti phase (largely made of Ti and solid solution-strengthened by Fe and Mo). It is shown that the design space of these

cermets is quite extensive and flexible, allowing either the creation of nearly 100% TiB nanoceramics for applications requiring hardness and strength on the one hand, or, cermets with an overall balance of strength and toughness, on the other hand. The advantages arise from several intrinsic attributes of the TiB ceramic phase. The high electron density of B–B bonds in these whiskers was found to give TiB high stiffness properties, which in turn adds to the strength and toughness.¹² The elastic modulus of monolithic TiB is in the range of 370–425 GPa^{13,14} and fracture toughness is ~ 4.5 MPa m^{1/2}.¹⁵ The hardness of the TiB phase is ~ 1800 kg/mm² (Hv).¹² However, the toughening of TiB needs to be engineered by the introduction of a metallic phase in the ceramic matrix.

From the processing perspective, an important principle governing the synthesis of TiB-based cermet materials is the in situ formation of TiB whiskers. Our previous research^{16,17} has shown that it is thermodynamically advantageous to use TiB₂ and Ti powders to form two-phase Ti–TiB composites according to the reaction: $\text{Ti} + \text{TiB}_2 \rightarrow 2\text{TiB}$. During reaction sintering, the orthorhombic TiB whiskers grow from the TiB₂ powders with B diffusing preferentially along B–B chains, through the length of the whiskers, to react with Ti. TiB is one of the three boride compounds that could form from the reaction between Ti and B, the others being TiB₂ and Ti₃B₄. However, when Ti and TiB₂ are reacted, it is found that TiB forms as whiskers with no residual Ti₃B₄ in the final product, even though it is an intermediate phase between Ti and TiB₂, in the Ti–B phase diagram.¹⁸

Toughening of the TiB ceramic phase needs the introduction of a metallic phase. However, the outstanding

^{a)}Address all correspondence to this author.

e-mail: ravi.chandran@utah.edu

DOI: 10.1557/jmr.2018.368

question is whether such a phase which can be simultaneously incorporated during in situ reaction sintering to form TiB. In the Ti–B binary system, however, only α -Ti is the stable phase at room temperature. α -Ti is an HCP phase with limited slip systems and is also subject to a loss of ductility or toughness in the presence of even very small amounts of interstitials such as O, N, and C.¹⁹ It is desirable, therefore, to stabilize the high temperature β -Ti phase down to room temperature, as this phase has a greater solubility for interstitials, along with an increased number of slip systems to produce ductility. The β -Ti metallic phase can be stabilized by the addition of elements that stabilize β phase in titanium.

The objective of this work is to design the TiB cermet compositions such that (i) they can be processed rapidly in one step by reaction sintering under electric field and (ii) a two-phase cermet is resulted, with the microstructure consisting of the ceramic boride phase and a substantial amount of metallic, ductile β -Ti phase. Additionally, extensive strength and toughness measurements have been made to assess the property merits of this class of cermets. The microstructural factors that control hardness, strength, and toughness are analyzed and discussed.

II. DESIGN AND EXPERIMENTAL PROCEDURE

A. Design of composition and processing

One of the challenges of processing TiB cermets is the lack of information about what should be the right composition and the processing temperature and/or pressures, which are desired to obtain a dense and homogeneous material. Although some rudimentary information is available from our earlier studies^{16,17} on Ti–TiB composites in the binary Ti–B system, the addition of

ternary or quaternary elements (Fe, Mo), to stabilize the β -Ti phase, must be guided by the extent of phase stability. In particular, in processing, we needed to determine the liquidus region, largely brought in by the addition of Fe, on the basis of low eutectic temperature (~ 1358 K), at Ti–33 wt% Fe, in the Ti–Fe system. Although we had used earlier the idea of liquid phase formation in synthesizing a ceramic, largely consisting of TiB (>85 vol%),²⁰ extensive liquid phase formation actually poses a problem, (due to oozing out of the liquid phase under small pressure in preliminary experiments) because the present target is to finalize cermets with 30–50% metallic toughening phase. This was found to be very critical because the seepage of the liquid phase between die gaps, under pressure, made the processing difficult in early trials.

To determine optimum processing condition for targeted compositions, CALPHAD calculations of phase stability regions in the Ti–B–Fe–Mo system were performed using Thermo-Calc software. The required thermodynamic data of Ti, B, Mo, and Fe were compiled and used as input data. Selected binary phase diagrams (Ti–Fe, Fe–B, Mo–B, and Ti–B) between the four components were simulated and verified with the corresponding experimental phase diagrams, to determine the binary interaction parameters. This detailed thermodynamic assessment is available elsewhere.²¹ These parameters were used as a basis, and, along with interpolations of higher order interaction parameters, the phase diagram calculations for the Ti–B–Fe–Mo system were performed. Figure 1 illustrates the pseudo-binary phase diagram of the Ti–B–Fe–Mo system. In constructing the diagram, the B composition was fixed at its stoichiometric composition for the TiB phase and the Fe content

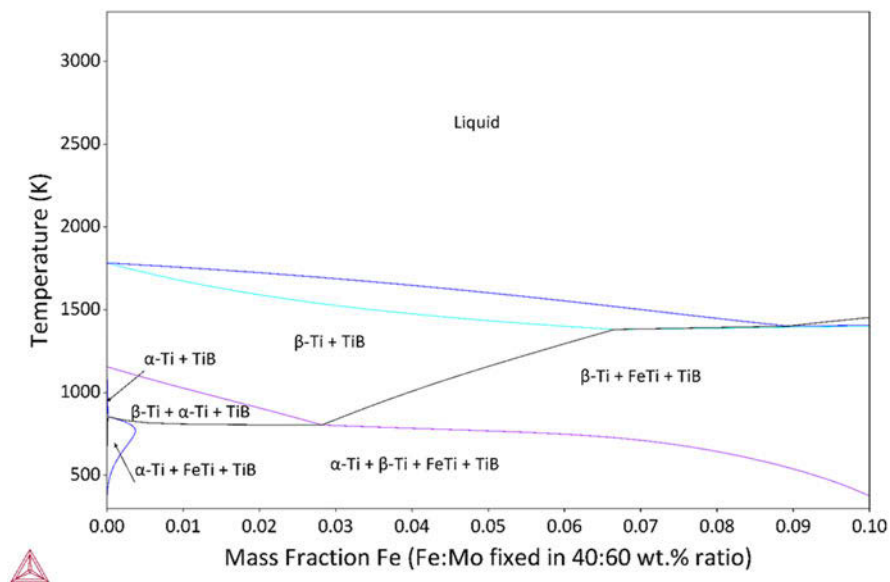


FIG. 1. Pseudo-binary Ti–B–Fe–Mo phase diagram with the B content is fixed at the stoichiometric TiB composition and the Fe:Mo weight ratio is fixed at 0.67.

TABLE I. Powder mixture compositions and calculated compositions for TiB-β-Ti cermets.

Target TiB (V_f)	TiB ₂ powder (w_f)	Ti powder (w_f)	Fe-Mo powder mixture (w_f)	Ti (V_f)	Actual TiB (V_f)	Relative density
0.5	0.296	0.628	0.076	0.51	0.49	0.996
0.6	0.355	0.575	0.07	0.43	0.57	0.995
0.7	0.41	0.526	0.064	0.33	0.67	0.998

(or the Mo content) were varied, with the Fe:Mo wt% ratio fixed at 0.6. However, the Fe:Mo ratio can be varied as desired in the calculations, but this will yield numerous compositions a detailed study of which is beyond the scope of the present work.

Figure 1 illustrates the pseudo-binary diagram (TiB-Fe/Mo) for the Ti-B-Fe-Mo system. The Fe/Mo composition of the cermets were designed (see Table I) to stay as close to the eutectoid point as possible such that partitioning of Fe/Mo in the β-Ti phase, and its stabilization, can occur over a wide temperature range. The sintering temperature was chosen explicitly to avoid the occurrence of the liquid phase in the β-Ti + TiB phase mixture during processing. This temperature needs to be as high as possible, while avoiding the liquid phase, to facilitate densification—the temperature 1473 K is sufficiently below the solidus line, for a range of Fe:Mo contents, and hence this was chosen as the processing temperature.

B. Materials

Cermets were made from the starting powders Ti, TiB₂, Fe, and Mo. The details of the powders used are Ti (99.7% pure; average particle size of 31 μm; Puris, West Virginia), TiB₂ (99.7% pure; average particle size of 14 μm; Momentive, New York), Fe powder (>99.9% pure; average particle size of 6 μm; Alfa Aesar, Massachusetts), and Mo powder (99.95% pure; average particle size of 11 μm; Alfa Aesar, Massachusetts).

While the Ti and TiB₂ contents were approximately fixed to yield a certain V_f of stoichiometric TiB and some V_f of the α-Ti phase, the Fe/Mo content, intended for the stabilization of the β-Ti phase, provides a very vast scope of compositions. For the present study, however, the wt% ratio of Fe:Mo powders was fixed as 0.67, to make scope manageable, although this ratio can be varied if desired. The powders were ball milled in containers under an inert atmosphere for 24 h. The mixture was loaded into a graphite die and was reaction-sintered in a 10-ton electric-field-activated sintering (EFAS) system (Thermal Technologies Model 10-4) at 1473 K. A heating rate of ~60 K/min and a hold time of 30 min at 1473 K under a pressure of 10 MPa were used. The power was turned off at the end of the isothermal hold period, allowing the sample to cool to near room temperature before removal from the die. The sample was cooled down under a ram pressure of 5 MPa. It

underwent a two-step cooling process. The cooling rate is 22.5 K/min in the range of 1473–1073 K. The power was cut off where temperature is below 1073 K, the sample was cooling naturally, and the cooling rate is about 60 K/min based on a typical temperature profile observed during cooling. Samples of size: 60 mm in diameter and 13 mm in thickness were made. From these, bars of size: 45 × 4 × 3 mm³ were cut by electric-discharge-machining for flexural and fracture toughness testing. At least 10 bars were tested for the flexural strength evaluation, and a minimum of 5 bars were used for fracture toughness test.

Three TiB-β-Ti cermet compositions were chosen, with target TiB vol% of 50, 60, and 70%, with the help of the calculated phase diagram. Densities of the sintered samples were measured using the Archimedes method. Metallographic samples were prepared by polishing with abrasive media and, to a fine finish with 0.5 μm colloidal silica, for optical and scanning electron microscopy and hardness measurements. X-ray diffraction (XRD) data were obtained on metallographically polished and unetched samples and these data were used to determine the phase content. An X-ray diffractometer (Rigaku, Miniflex 600, Japan) was used to obtain the diffraction pattern data with a scan rate of 0.5°/min. For SEM microscopy, the samples were etched with Kroll's reagent. Standard test methods^{22,23} for flexural strength (ASTM C1161-13) and fracture toughness (ASTM C1421-10) testing of advanced ceramics in the four-point bend configuration were used. The test bars were loaded at displacement rates of 0.5 and 0.18 mm/min, for flexural and fracture testing, respectively.

C. Estimation of TiB volume fraction

Using the method developed by Sahay et al.,¹⁶ the relative volume fractions of Ti and TiB phases were computed from the integrated intensities of selected peaks in the XRD pattern of each cermet composition. Assuming a generally two-phase microstructure, this approach uses the direct comparison of the integrated intensity of a strong TiB peak with that of a Ti peak. The volume fraction of TiB (V_f) can be written as

$$V_f = \frac{R_{Ti} I_{TiB}}{R_{Ti} I_{TiB} + R_{TiB} I_{Ti}} \quad (1)$$

where I is the integrated intensity of the (hkl) peak. The parameter R , for each phase, is given by

$$R = \frac{|F_{hkl}|^2 pL}{V_0} \quad (2)$$

where V_0 is the volume of the unit cell, F_{hkl} is the structure factor, p is the multiplicity factor, and L is the Lorentz polarization factor. The calculation of these parameters was shown in the previous work.²⁴ The

volume fractions of phases in the present cermets, so determined, are given in Table I. Hereafter the cermets will be referred to on the basis of actual TiB V_f , given in Table I.

III. RESULTS AND DISCUSSION

A. Processing

Density measurements verified that sintered samples were nearly 100% dense (Table I) on the basis of theoretical values, which is also confirmed by the lack

of porosity visible in micrographs. The ram displacement and operating power, as recorded using the EFAS processing for each cermet composition at 1473 K are shown in Fig. 2. The behavior of ram displacement, with time during sintering, is nearly identical for the three cermets and indicates that the densification behavior is similar for the three compositions investigated. The actual densities were measured physically and reported as relative densities in Table I. However, the steady-state power during densification was slightly higher for the cermet with the higher metal content.

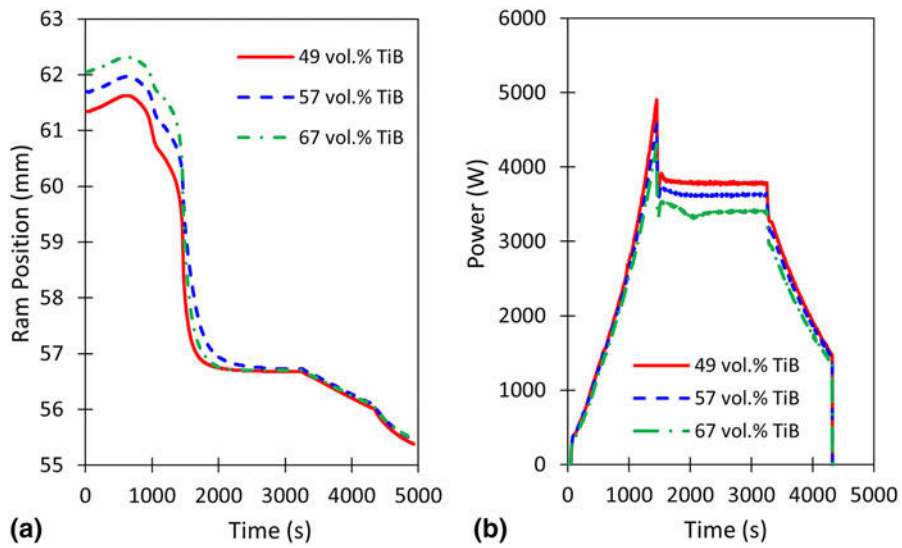


FIG. 2. The variation in (a) ram displacement and (b) power during EFAS of the cermets.

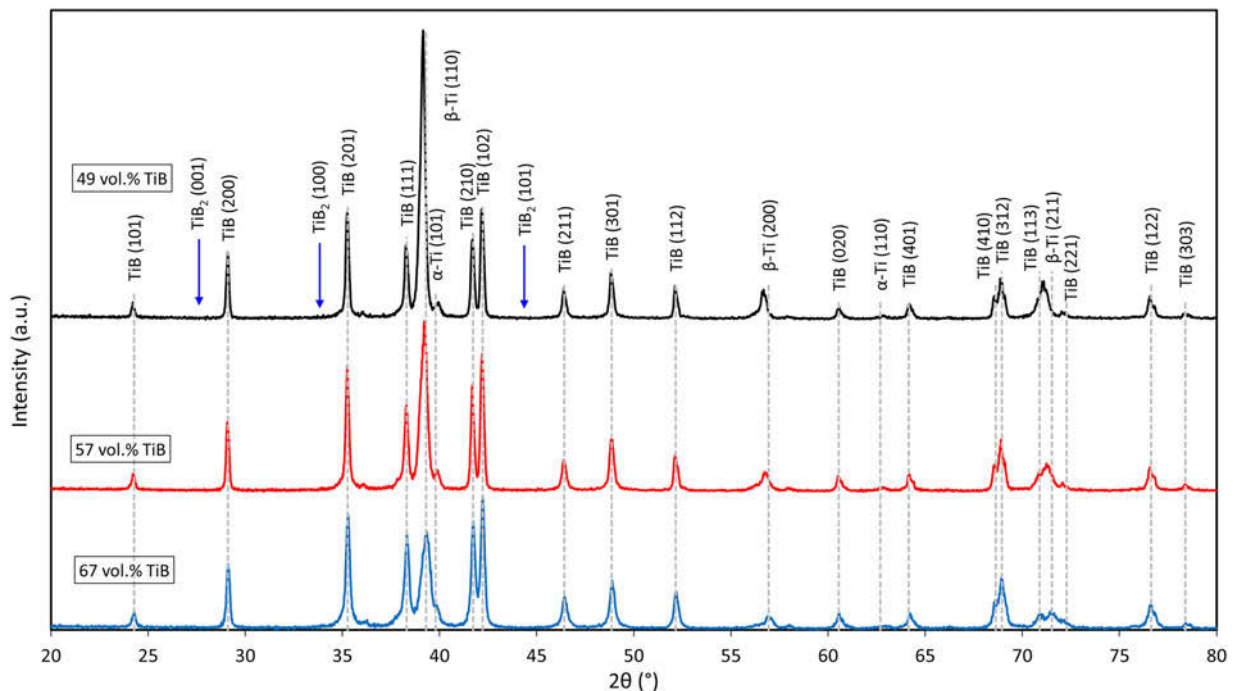


FIG. 3. XRD showing the presence of phases after EFAS at 1473 K for TiB cermet compositions.

B. X-ray diffraction data

The formations of TiB and β -Ti phases, during reaction sintering of powders and as characterized by XRD data, are demonstrated in Fig. 3. From the XRD patterns, it is evident that sintering at 1473 K for 30 min was sufficient to achieve full reaction in all of the compositions. The XRD patterns confirm the two-phase (β -Ti and TiB) microstructure and the absence of any unreacted TiB₂. It can also be seen that a nearly full β -stabilization was achieved, as evidenced by the strong (110) β -Ti peaks, although there is a small visible presence of α -Ti, possibly arising due to a combination of the relatively slow cooling rate (unlike quenching, please see Sec. II. B) after sintering and the Fe/Mo content being in a metastable range of Mo equivalence. The relative amount of α/β phases in a beta alloy composition depends on the Mo equivalence. The estimated $[\text{Mo}]_{\text{eq}}$ of the β -Ti phases in the 49, 57, and 67 vol% TiB cermets are 24%, 28%, and 33%, respectively, which means that in all cermets, the compositions of the beta phases in the cermets are in the metastable region of β -Ti alloys.²⁵

C. Microstructure

Microstructures of the sintered samples are presented in Fig. 4. All the cermets reveal a general two-phase structure, with the TiB phase being present largely as the continuous phase in the matrix. The TiB phase itself, in each cermet composition, is made of a bundle of TiB whiskers tightly packed together [Figs. 4(a), 4(c), and 4(e)], with some islands of the β -Ti phase within each bundle, as visible in high magnification images [Figs. 4(b), 4(d), and 4(f)]. The β -Ti in the cermets is present in two morphologies—one is the large islands between the bundles of TiB and the other is the smaller islands within the bundles. By design, there are larger and relatively higher volume fractions of the β -Ti phase in the compositions with lower TiB volume fractions. In all the cermets, however, a significant amount of “in-growth” of TiB whiskers into the beta phase regions is also evident. This seems to occur to a greater degree in the cermet with the highest TiB volume fraction [Fig. 4(f)]. This growth is partly because of the reduced volume fraction of the β -Ti phase in this cermet, and consequently the relatively reduced mean-free-distance. Therefore, the larger β -Ti islands, in the high volume fraction TiB cermet, is heavily reinforced by the in-growing TiB whiskers.

The distributions of β -stabilizing elements, resulting from in situ formations of TiB whiskers, were also investigated. Using wavelength-dispersive-spectroscopy (WDS), the spatial distributions of B, Fe, and Mo were mapped and are shown in Figs. S1(a)–S1(c), given in the Supplementary Material. Figure S1(a) shows the typical distribution of B within the TiB phase—the light regions indicate the presence of B and the dark regions indicate the absence of B, relatively. It is evident that there is no B within the large β -Ti islands, as well as within the smaller islands within in TiB. This is consistent with the Ti–B binary phase diagram, showing almost no solubility of B in α/β Ti phases. It is therefore clear that nearly all of B is in the form of TiB phase. However, Fe and Mo are distributed differently between the ceramic and metal phase. The light regions in (b) and (c) suggest that Fe and Mo are essentially concentrated within the β -Ti phase forming the large as well as the small islands. Although Fe seems to be exclusively concentrated within the β -Ti phase, there appears to be some distribution of Mo within the TiB regions, possibly, forming a ternary boride of stoichiometry $\text{Ti}_x\text{Mo}_{1-x}\text{B}$, where “x” the mole fraction of Ti atoms within the boride. However, interestingly in Fig. S1(c), the large TiB whiskers that seem to grow into the large β -Ti islands appear to be darker than the major bundles of TiB whiskers, and hence appear to have a much less concentration of Mo in them. A more detailed analysis of these two different forms of spatial distribution of Mo, within the TiB phases, is beyond the scope of the present study.

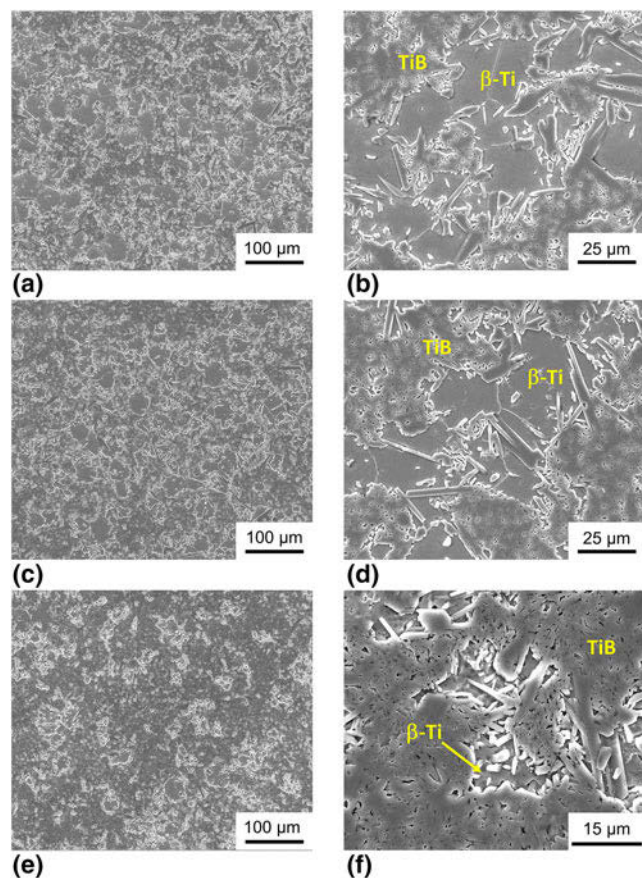


FIG. 4. SEM micrographs of (a, b) 49 vol% TiB, (c, d) 57 vol% TiB, and (e, f) 67 vol% TiB cermet samples.

D. Mechanical properties

1. Hardness variation

The Vickers hardness of TiB is around 1800 kg/mm^2 .¹² The Vickers hardness values of β -Ti phases in the cermets could not be measured in a way unaffected by the surrounding and grown-in TiB phases, especially at the load (1 kg) used in the present hardness measurements. This is because the β -Ti phase size was smaller than the hardness indentation size. The distribution of hardness values is presented in the form of cumulative probability plot in Fig. 5. Vickers hardness values ranged from 645 to 932, 682–1131, and 831–1391 kg/mm^2 , for the 49%, 57%, and 67% TiB cermets, respectively. The increased hardness levels in the higher TiB volume fraction cermet is evidently due to the increased spatial presence of TiB in the microstructure, relative to the other cermets. However, the hardness levels overlapped between the cermets, indicating that a hardness level is a reflection of the influence of both the TiB and the β -Ti phases in the cermets. It should also be noted that in random hardness measurements, the sizes of the indentations, relative to the size scale of the phases in the microstructure, as well as the location of indentation will influence the hardness value. The largest size of the hardness indentation (lowest hardness) was about $40 \mu\text{m}$ which is larger than the average mean-free-intercept distance of the β -phase ($\sim 30 \mu\text{m}$). Additionally, often the beta phase has TiB whiskers growing into it, from the bulk TiB phase in the microstructure. Hence, the hardness measurements represent some average of the hardness of each phase and this average depends on where the indentation is made, which is not known a priori because Vickers hardness measurements are location-blind with respect to the microstructure. However, from a statistical representation of hardness data, it may be possible to back-calculate the hardness of the β -phase in each cermet composition and assess how this impacts the overall hardness of the cermets. It was found that the hardness distribution can be well described by a Weibull type function:

$$P = 1 - \exp \left[-C \left\{ \frac{H - H_{\beta}}{H_{\text{TiB}} - H_{\beta}} \right\}^n \right], \quad (3)$$

where H is the hardness of a random measurement, and H_{TiB} and H_{β} are the hardness values of the TiB and the β -Ti phase, respectively. Figure 5 illustrates the experimental hardness distributions, compared with the calculations from the Weibull function [Eq. (3)], by taking $H_{\text{TiB}} = 1800 \text{ kg/mm}^2$. To achieve the best possible fit to the distribution of hardness data, the required H_{β} values were found to be 300, 400, and 700 kg/mm^2 in 49, 57, and 67% TiB cermets, respectively. It is therefore evident that the higher average hardness of the β -Ti phase produces relatively higher values of hardness distribution,

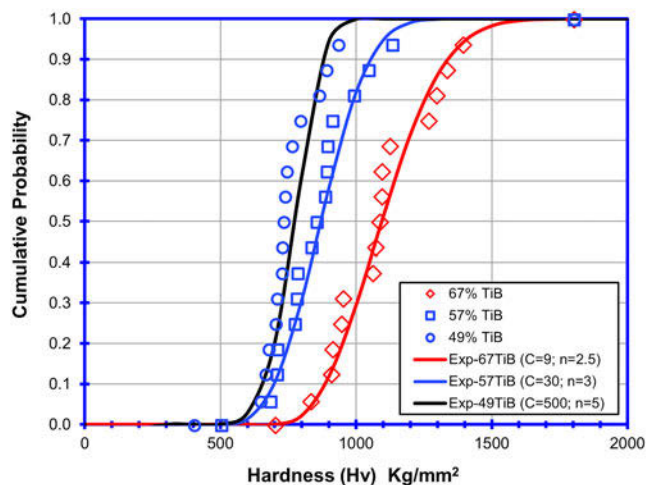


FIG. 5. Distribution of Vickers hardness values in TiB cermets.

in the 67% TiB cermet, compared to the other cermets. It is not clear why the hardness of the β -Ti phase is lower in the cermets with relatively lower TiB content—but this can be attributed to the change in composition of the β -Ti phase in these cermets.

2. Flexure strength

The flexural strengths of the three cermet compositions are presented in Figs. 6(a)–6(c). The flexure strength ranges were 875–1013, 666–936, and 780–981 MPa for the 49, 57, and 67 vol% TiB cermets, respectively. These strength values are in the medium-to-high range, from the perspective of potential industrial cermets, under development, some examples of which are presented in Table II. The figures also illustrate the lines, which are fit to the data according to the two-parameter Weibull distribution:

$$P_f = 1 - \exp \left[- \left\{ \frac{\sigma}{\sigma_0} \right\}^m \right], \quad (4)$$

where P_f is the probability of failure, m is the Weibull modulus, and σ_0 is the characteristic strength corresponding to $P_f = 0.632$. While the characteristic strength values are largely similar (varying from 862 to 953 MPa) to each other, Weibull moduli shows a strong variation (m varying from 8.6 to 24.8) with cermet composition. However, a specific pattern, in terms of vol% of the TiB phase, or that of the β -Ti phase, is not evident.

The lack of a correlation of the strength pattern in the Weibull plots, with cermet composition, appears to be related to the effect of random inclusions on strength. The type and the size of the inclusion particle, as well as their location below the tensile surface during bending, contributed to observed variability of strength results. SEM analysis of fracture surfaces of each flexure sample

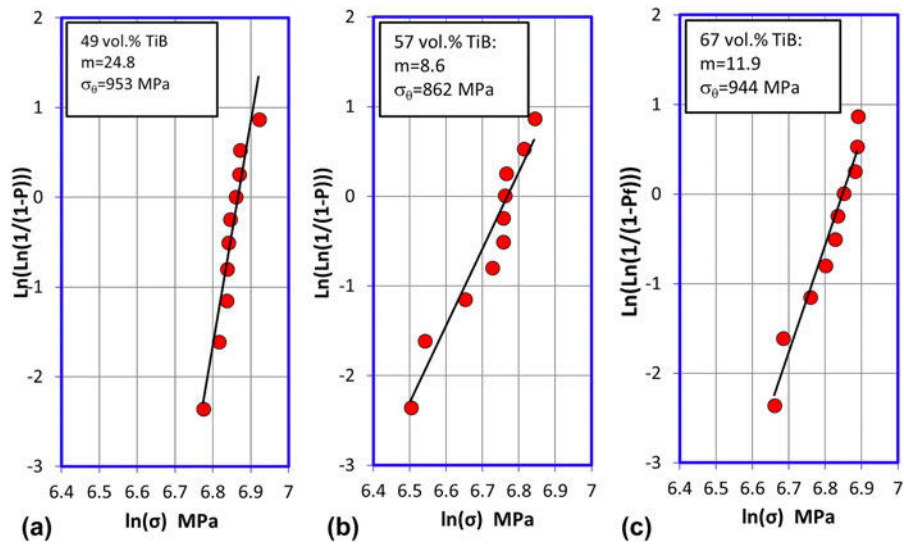


FIG. 6. (a–c) show the flexural strength, Weibull modulus (m), and characteristic strength (σ_0) results for TiB cermet compositions of 49%, 57%, and 67% TiB, respectively.

TABLE II. Comparison of mechanical properties of the present cermets with other cermets in the literature.

Cermet composition	Volume fraction ceramic phase	Vickers hardness (kg/mm ²)	Flexural strength (MPa)	Fracture toughness (MPa m ^{1/2})	Reference
WC-Co	0.7	1870	1234	16	31
WC-Co	0.69	1845	1180	16.9	32
WC-FeAl	0.7	653 ^a	950	18	33
TiC-FeAl	0.7	832 ^a	1034	18	34
TiB-β-Ti	0.49	752	953	17.8	This research
TiB-β-Ti	0.57	857	862	15.4	This research
TiB-β-Ti	0.67	1090	944	10.5	This research

^aConverted from Rockwell HRA values.

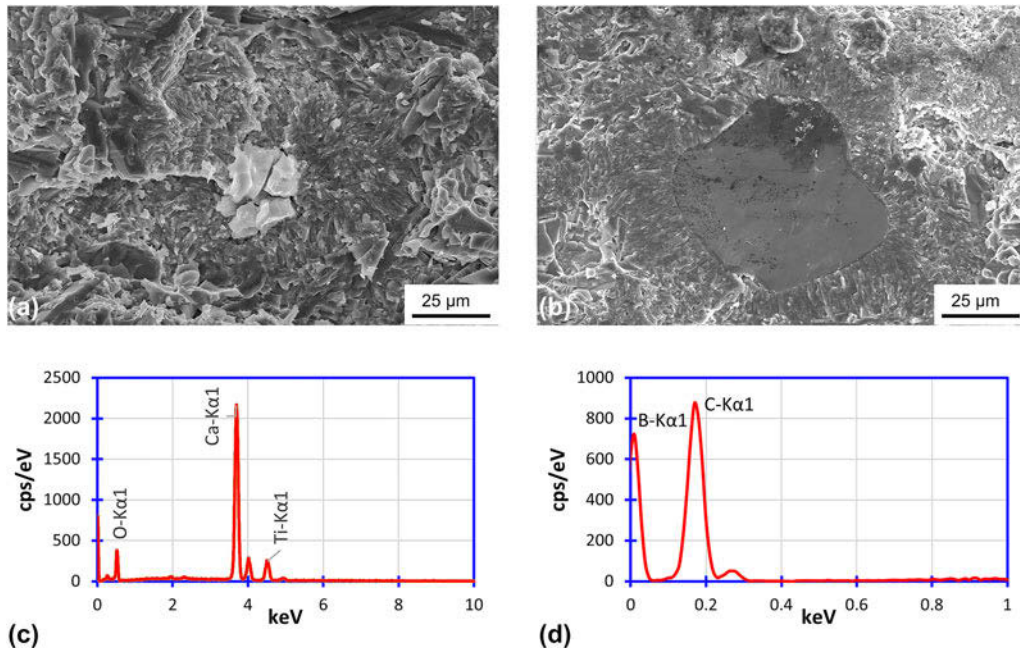


FIG. 7. SEM micrographs of (a) Ca–O and (b) B–C inclusion particles causing failure in strength tests. The corresponding EDS characterizations are shown in (c) and (d).

revealed the presence of inclusion particles, at the fracture origins, as shown in Fig. 7. Particles of CaO-type [$\sim 10\text{--}30\ \mu\text{m}$ in size; Fig. 7(a)] as well as relatively large particles enriched in B and C [$\sim 30\text{--}50\ \mu\text{m}$ in size; Fig. 7(b)], were found to be the sources of fracture initiation in the flexure samples. Energy dispersive spectroscopy (EDS) analysis of these inclusions is shown in Figs. 7(c) and 7(d). The CaO inclusions [Fig. 7(a)] probably formed from the impurities in the source powders. In particular, Ca and O are considered to have originated from the high purity titanium powders used in the synthesis. However, atomic absorption spectroscopy

(AAS) analysis of the Ti powder failed to confirm in the presence of Ca above the noise level. This may be the case if CaO had been present already as isolated inclusions within certain Ti powder particles, which, by chance, might not have entered the sample used in the AAS analysis. In the production of low-oxygen Ti powder, Ca is used as a deoxidant. Therefore, the likely source of Ca is the deoxidation step that was necessary to get low oxygen Ti powder and this Ca is likely to be present as CaO in the source powder. On the other hand, the source of B/C in the large particles [Fig. 7(b)] is not clear. Although there are sufficient Ti

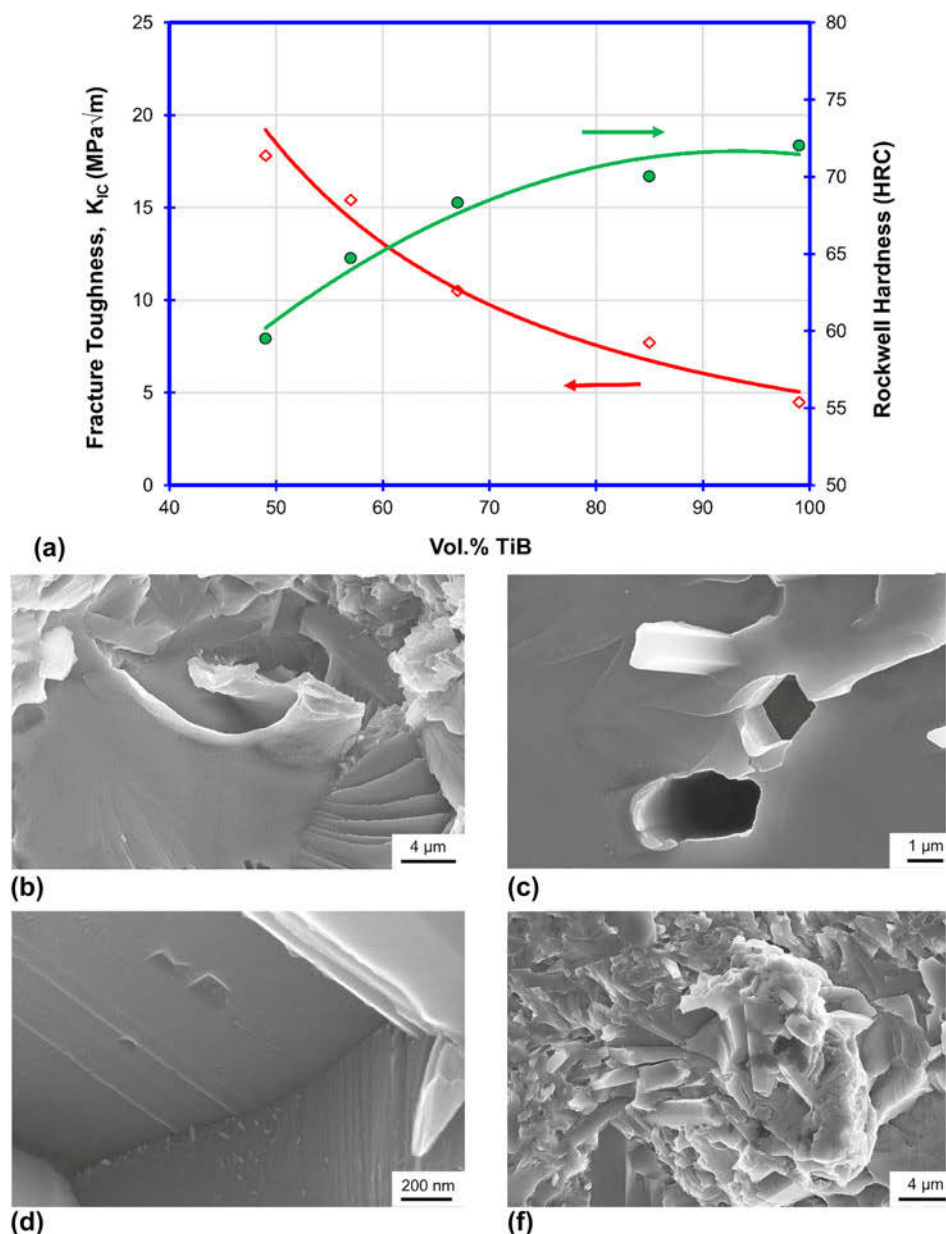


FIG. 8. (a) Fracture toughness and hardness data as a function of TiB content in the cermet. The increase in toughness, at low TiB content, is due to the presence of β -Ti phase. Although the beta phase appear to fracture largely in a cleavage manner (b & d), there are instances of pull-out of TiB whiskers (c), and crack deflection by β -Ti regions (f), which seem to contribute to the toughness of cermets.

particles in the initial mixture to react and convert all the B in the TiB_2 particles into TiB, there could be two possibilities that lead to deviations from this: (i) there might have been some residual B_4C in the TiB_2 source powder, arising from the powder production route or (ii) some residual B present in TiB_2 might have reacted with C in the lining of graphite dies used in processing. Nevertheless, when these impurities and inclusions are eliminated and high quality raw powders are used in the synthesis, one can expect a much higher strength level in all the cermets.

3. Fracture toughness

Fracture toughness (K_{IC}) values, determined using single-edge-cracked beam specimens in bending, are illustrated as a function of the vol% of TiB content in Fig. 8(a). The corresponding Rockwell hardness (HRC) values are also plotted using the right axis. A toughness of about $18 \text{ MPa m}^{1/2}$ was achieved with the 49 vol% TiB samples while still maintaining a hardness of about 58 R_C , which is comparable to hardened steels. The hardness increases with increasing TiB content up to about 70 R_C while still maintaining a toughness of about $7.7 \text{ MPa m}^{1/2}$. These data are for the sample with 85 vol% TiB, for TiB with 15 vol% metallic phase, the results of which are reported elsewhere.²⁶ TiB samples with 99 vol% TiB were tested in a previous study²⁷ and found to have the toughness of $\sim 5.0 \text{ MPa m}^{1/2}$ and a hardness of $\sim 72 R_C$. These values represent the terminal values of hardness and toughness for the TiB phase.

Figure 8 depicts the fracture behavior of TiB- β -Ti cermets during the propagation of a crack through the bulk of the sample. Figure 8(b) shows the cleavage of β -Ti, although the phase itself might have deformed with some plasticity before cleavage; Figure 8(c) shows pull-out of the TiB whiskers that had grown into the β -Ti phase; Figure 8(d) depicts a grain boundary where β -Ti cleavage planes meet; and Fig. 8(e) depicts a protruding mass of the matrix and the whisker material which appears to form when the fracture path tries to bypass the β -Ti phase by fracturing along the TiB- β -Ti interface, which was further confirmed by sidewise examination of fracture bars. The processes observed in Figs. 8(b)–8(e) will consume some energy during fracture, toughening the material relative to a 100% TiB material in which these processes are absent. In general, increased toughness in TiB cermets can be attributed to the operation of these energy dissipation processes as a result of the ductile β -Ti phase, as seen in many brittle-matrix-ductile-particle composites^{28–30} and WC-Co cermets.⁹

4. Comparison with other cermets

The mechanical properties of the TiB cermets, evaluated in this study, are compared with the similar

mechanical property data of other cermets that have been reported in the literature, some of which are summarized in Table II. Only mechanical property data for cermets with 67% hard/ceramic phase are taken for comparison with the TiB cermet with 67 vol% TiB. Data for other cermets at lower contents of the hard phase are not commonly available, as these are seldom studied. Although the hardness and flexural strengths of 67 vol% cermet of the present study is lower than that of WC-Co cermets, it is noteworthy that it compares favorably well with WC-FeAl and TiC-FeAl cermets, in terms of these properties. The fracture toughness is lower, and this is possibly due to the cleavage fracture of the β -Ti phase, whereas the FeAl metallic phase in the WC-FeAl and TiC-FeAl cermets were found to exhibit ductile fracture.

One reason for the superiority of WC-Co, in almost all aspects, with respect to the present system, is that it is a highly optimized material, with nearly a century of study and development. Specifically, the WC grains are much smaller ($\sim 2\text{--}4 \mu\text{m}$) giving a high hardness, and the Co phase is highly ductile giving a high level of toughness, both of which have been worked out after a long time of research and development. In the first ever attempts of making and evaluating the present cermets, the TiB phase is significantly coarse ($>50 \mu\text{m}$) and clustered as a network, while the β -Ti phase is present as islands, with minimal ductility. Nevertheless, it appears that there is significant potential for further refinements in alloy design and processing, to increase, principally, the ductility of the β -Ti phase. In view of the rapid processing advantage (a reaction sintering temperature of $\sim 1473 \text{ K}$ for 30 min) of the present class of cermets, further research to optimize and improve properties is clearly warranted.

IV. CONCLUSIONS

(1) A material design and processing approach, to synthesize a new class of cermets based on titanium boride (TiB) are presented. Cermet compositions in the Ti-B-Fe-Mo system with 49, 57, and 67 vol% boride phases were successfully synthesized to full density at a relatively low temperature in a single step, achieving equilibrium phases and microstructure.

(2) Microstructures revealed the uniform distribution of titanium boride and metallic β -Ti phases with the stabilization of the metal phase enabled by the Fe/Mo additions.

(3) Average Vickers hardness was evaluated at 752, 857, and 1090 kg/mm^2 for the 49, 57, and 67 vol% TiB samples, respectively. The hardness exhibited significant variation due to the spatial randomness of the indentations in the two-phase microstructure. A Weibull-type exponential function has been shown to describe the spatial variation in hardness, very well.

(4) A range of flexural strength between 780 and 981 MPa was observed in the cermet containing 67 vol% of the TiB phase. There was no evident order of strengthening, with respect to the proportions of the brittle and ductile phases in the cermets. It was found that the intrinsic strength of the TiB phase combined with that of reinforcing metal phase added to the overall strength while large inclusion particles deteriorated strength.

(5) The strength properties of cermets are somewhat limited by the unexpected formation Ca–O and B–C inclusion particles, with the impurity elements coming from source powders. Elimination of these particles from TiB– β Ti cermets could improve the mechanical properties.

(6) Fracture toughness was evaluated as 10.5, 15.4, and 17.8 MPa m^{1/2} for the 49, 57, and 67 vol% compositions, respectively. Although the metallic phase fractured in a cleavage manner, the toughness increased as the metallic content was increased in the cermet.

(7) Currently, the toughness is limited by the cleavage fracture of the metallic beta-titanium phase. Further optimization of composition and processing, to enable failure by ductile rupture, will lead to a significantly increased fracture toughness values for these cermets.

ACKNOWLEDGMENTS

The research, largely performed M.S. thesis research of the first author, was supported by the National Science Foundation, the program on Designing Materials to Revolutionize our Engineering Future (DMREF), through the grant CMMI-1435758. The assistance provided by Dr. Tony Sanders, Dr. Mark Koopman, Somnaang Rou, Ahmed Degnah, and Richard Laroche is acknowledged.

REFERENCES

- H.E. Exner: Physical and chemical nature of cemented carbides. *Int. Met. Rev.* **24**, 149 (1979).
- P. Ettmayer: Hardmetals and cermets. *Annu. Rev. Mater. Sci.* **19**, 145 (1989).
- D. Moskowitz and J. Humenik: TiC-based cermets for cutting applications. *Mod. Dev. Powder Metall.* **14**, 307 (1985).
- I.W.M. Brown and W.R. Owers: Fabrication, microstructure and properties of Fe–TiC ceramic–metal composites. *Curr. Appl. Phys.* **4**, 171 (2004).
- R. Subramanian and J.H. Schneibel: FeAl–TiC and FeAl–WC composites—Melt infiltration processing, microstructure and mechanical properties. *Mater. Sci. Eng., A* **244**, 103 (1998).
- S.Y. Zhang: Titanium carbonitride-based cermets: Processes and properties. *Mater. Sci. Eng., A* **163**, 141 (1993).
- J. Gurland: New scientific approaches to development of tool materials. *Int. Met. Rev.* **33**, 151 (1988).
- S.L. Sigl and H.F. Fischmeister: On the fracture toughness of cemented carbides. *Acta Metall.* **36**, 887 (1988).
- K.S. Ravichandran: Fracture toughness of two-phase WC–Co cermets. *Acta Metall. Mater.* **42**, 143 (1994).
- M. Humenik, Jr. and N.M. Parikh: Cermets: I, fundamental concepts related to micro-structure and physical properties of cermet systems. *J. Am. Ceram. Soc.* **39**, 60 (1956).
- N.M. Parikh and M. Humenik, Jr.: Cermets: II, wettability and microstructure studies in liquid-phase sintering. *J. Am. Ceram. Soc.* **40**, 315 (1957).
- S. Madtha, C. Lee, and K.S. Ravi Chandran: Physical and mechanical properties of nanostructured titanium boride (TiB) ceramic. *J. Am. Ceram. Soc.* **91**, 1319–1321 (2008).
- R.R. Atri, K.S. Ravichandran, and S.K. Jha: Elastic properties of in situ processed Ti–TiB composites measured by impulse excitation of vibration. *Mater. Sci. Eng., A* **271**, 150 (1999).
- K.B. Panda and K.S. Ravi Chandran: First principles determination of elastic constants and chemical bonding of titanium boride (TiB) on the basis of density functional theory. *Acta Mater.* **54**, 1641 (2006).
- S. Nakane, Y. Takano, M. Yoshinaka, K. Hirota, and O. Yamaguchi: Fabrication and mechanical properties of titanium boride ceramics. *J. Am. Ceram. Soc.* **82**, 1627 (1999).
- S.S. Sahay, K.S. Ravichandran, and R. Atri: Evolution of microstructure and phases in in situ processed Ti–TiB composites containing high volume fractions of TiB whiskers. *J. Mater. Res.* **14**, 4214 (1999).
- S. Madtha and K.S. Ravi Chandran: Reactive-sinter-processing and attractive mechanical properties of bulk and nanostructured titanium boride. *J. Am. Ceram. Soc.* **95**, 117 (2012).
- Titanium–Boron System: *ASM Handbook: Alloy Phase Diagrams*, Vol. **3** (ASM International, Materials Park, Ohio, 1992); p. 440.
- H. Conrad: Effect of interstitial solutes on the strength and ductility of titanium. *Prog. Mater. Sci.* **26**, 123 (1981).
- J. Du and K.S. Ravi Chandran: Formation of bulk titanium boride (TiB) nano-ceramic with Fe–Mo addition by electric-field-activated-sintering. *J. Am. Ceram. Soc.* **100**, 5450 (2017).
- V. Jindal and K.S. Ravi Chandran: *Thermodynamic Assessment of Ti–B–Fe–Mo Quaternary System* (Department of Metallurgical Engineering, University of Utah, Salt Lake City, 2018). (unpublished research).
- ASTM International: ASTM C1161-13 Standard test method for flexural strength of advanced ceramics at ambient temperature. ASTM Stand. B. C. 1 (2013); pp. 1–19.
- ASTM International: ASTM C1421-10 Standard test methods for determination of fracture toughness of advanced ceramics at ambient temperature. ASTM Stand. B.I. 1 (2011).
- K. Panda and K.S. Ravi Chandran: Synthesis of ductile Ti–TiB composites with β -Ti alloy matrix. *Metall. Mater. Trans. A* **34**, 1371 (2003).
- J.D. Cotton, R.D. Briggs, R.R. Boyer, S. Tamirisakandala, P. Russo, N. Shchetnikov, and J.C. Fanning: State of the art in beta titanium alloys for airframe applications. *JOM* **67**, 1281 (2015).
- J. Du and K.S. Ravi Chandran: CALPHAD-guided alloy design and processing for high strength and high toughness in titanium boride (TiB) nanoceramic system. *Acta Mater.* (2018). (submitted to).
- J. Du and K.S. Ravi Chandran: Department of Metallurgical Engineering, University of Utah, Salt Lake City, Utah (unpublished research).
- K.S. Ravichandran: A survey of toughness in ductile phase composites. *Scr. Metall. Mater.* **26**, 1389 (1992).
- M.A. Przystupa and T.H. Courtney: Fracture in equiaxed two phase alloys: Part II. Fracture in alloys with isolated plastic particles. *Metall. Trans. A* **13**, 881 (1982).
- B.D. Flinn, M. Rühle, and A.G. Evans: Toughening in composites of Al₂O₃ reinforced with Al. *Acta Metall.* **37**, 3001 (1989).

31. J.L. Chermant and F. Osterstock: Fracture toughness and fracture of WC-Co composites. *J. Mater. Sci.* **11**, 1939 (1976).
32. J.R. Pickens and J. Gurland: The fracture toughness of WCCo alloys measured on single-edge notched beam specimens pre-cracked by electron discharge machining. *Mater. Sci. Eng.* **33**, 135 (1978).
33. J.H. Schneibel, C.A. Carmichael, E.D. Specht, and R. Subramanian: Liquid-phase sintered iron aluminide-ceramic composites. *Intermetallics* **5**, 61 (1997).
34. R. Subramanian, J.H. Schneibel, K.B. Alexander, and K.P. Plucknett: Iron aluminide-titanium carbide composites by pressureless melt infiltration—Microstructure and mechanical properties. *Scr. Mater.* **35**, 583 (1996).

Supplementary Material

To view supplementary material for this article, please visit <https://doi.org/10.1557/jmr.2018.368>.